

Hysteresis in a quantized superfluid atomtronic circuit

Stephen Eckel¹, Jeffrey G. Lee¹, Fred Jendrzejewski¹, Noel Murray², Charles W. Clark¹, Christopher J. Lobb¹, William D. Phillips¹, Mark Edwards² & Gretchen K. Campbell¹

¹*Joint Quantum Institute, National Institute of Standards and Technology and University of Maryland, Gaithersburg, Maryland 20899, USA*

²*Department of Physics, Georgia Southern University, Statesboro, Georgia 30460-8031, USA*

Atomtronics ^{1,2} is an emerging interdisciplinary field that seeks new functionality by creating devices and circuits where ultra-cold atoms, often superfluids, play a role analogous to the electrons in electronics. Hysteresis is widely used in electronic circuits, e.g., it is routinely observed in superconducting circuits ³ and is essential in rf-superconducting quantum interference devices [SQUIDs] ⁴. Furthermore, hysteresis is as fundamental to superfluidity ⁵ (and superconductivity) as quantized persistent currents ⁶⁻⁸, critical velocity ⁹⁻¹⁴, and Josephson effects ^{15,16}. Nevertheless, in spite of multiple theoretical predictions ^{5,17-19}, hysteresis has not been previously observed in any superfluid, atomic-gas Bose-Einstein condensate (BEC). Here we demonstrate hysteresis in a quantized atomtronic circuit: a ring of superfluid BEC obstructed by a rotating weak link. We directly detect hysteresis between quantized circulation states, in contrast to superfluid liquid helium experiments that observed hysteresis directly in systems where the quantization of flow could not be observed ²⁰ and indirectly in systems that showed quantized flow ^{21,22}. Our techniques allow us to tune the size of the hysteresis loop and to consider the fundamental excitations that accompany hysteresis. The

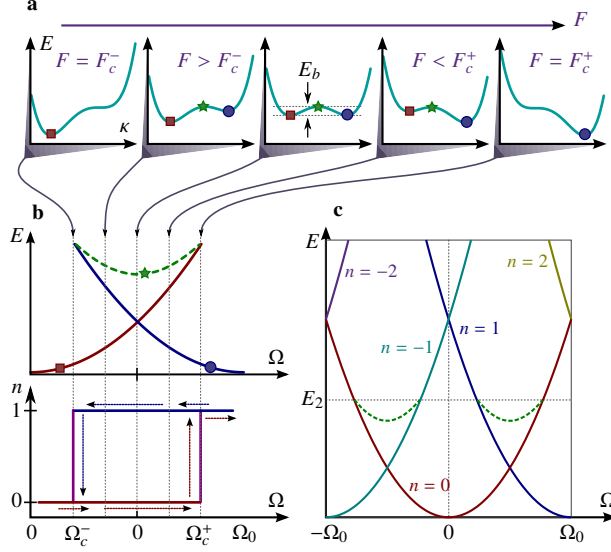


Figure 1: Origin of hysteresis. **a**, A schematic of the energy landscape of a hysteretic system. As a function of an order parameter κ , the energy can have local minima (■,●), which represent stable states, separated by a local maximum (★), which forms an energy barrier E_b . This landscape is shown for five values of the applied field F (for superfluidity, $F \rightarrow \Omega$, the rotation rate of the trap). **b**, Plotted as a function of Ω for a superfluid, the energy of the minima (solid) and maximum (dashed) form a swallowtail (upper), which exhibits hysteresis (lower). **c**, This swallowtail structure is periodic in Ω_0 ; states above E_2 are unstable.

results suggest that the relevant excitations involved in hysteresis are vortices and indicate that dissipation plays an important role in the dynamics. Controlled hysteresis in atomtronic circuits may prove to be a crucial feature for the development of practical devices, just as it has in electronic circuits like memory, digital noise filters (e.g., Schmitt triggers), and magnetometers (e.g., SQUIDs).

Hysteresis is a general feature of systems where the energy has two (or more) local minima

separated by an energy barrier. A schematic of this type of energy landscape is shown in Fig 1a. A canonical example of hysteresis is the Landau theory of ferromagnetism ²³, where the order parameter κ is the magnetization, and $E(\kappa)$ has two minima (stable states) corresponding to the magnetization being aligned or anti-aligned to the applied magnetic field. In the case of a BEC in a ring-shaped trap, these minima represent stable flow states of the system, and their energies depend on the applied rotation rate of the trap, Ω (here, this rotation is created using a rotating repulsive perturbation). With no interatomic interactions, there is only one minimum in the energy landscape of the BEC. With the addition of interactions, an energy barrier can appear creating two (or more) stable flow states. This barrier stabilizes the flow, making the BEC a superfluid ^{5,24}.

The energy of the barrier is not generally known for superfluid systems; depending on the parameters of the system it could be related to the energy required to create elementary excitations such as phonons, solitons, or vortices. On the other hand, the stable states are well known. Rotation of a superfluid in a ring is characterized by a quantized rotation frequency $n\Omega_0$, where n is the winding number, $\Omega_0 = \hbar/(mR^2)$ is the rotational quantum, \hbar is Planck's constant divided by 2π , m is the mass of an atom, and R is the mean radius of the trap. The energy of the superfluid in the frame that rotates with the trap depends on the relative velocity between the superfluid and the trap ^{5,24}, and the energy is proportional to $(n - \Omega/\Omega_0)^2$.

Any ring-shaped superfluid *must necessarily* exhibit both hysteresis and a critical rotation rate Ω_c^\pm (or, equivalently, a critical velocity), because all these effects fundamentally arise from the energy barrier that creates superfluidity. To understand this, we plot the energy of the stable states

and the energy barrier as a function of Ω . Fig. 1b shows this *swallowtail* energy structure. If the system begins in $n = 0$, the flow is stable until $\Omega = \Omega_c^+$, where the energies of the $n = 0$ state and the barrier are equal. At this point, the $n = 0$ state is no longer stable and a transition occurs to $n = 1$, which has lower energy. If Ω is now decreased, this state is stable until $\Omega < \Omega_c^-$, where the flow changes. Thus, a typical hysteresis loop is traced, as shown in the bottom of Fig. 1b. Note that while the Ω_c^\pm are the same relative to the superfluid flow, they are generally different in the lab frame and thus appear as hysteresis. Furthermore, in the hysteretic case, the Ω_c^\pm are different from a more general definition of critical rotation (or velocity) that involves the onset of dissipation or the creation of excitations. At Ω_c^\pm , the hysteretic system may create excitations or experience dissipation, but both cease after the transition is made. Measurement of a hysteresis loop, in addition to measuring Ω_c^\pm , shows an important feature of the underlying energy landscape: the system has at least two stable states. Bi-stability of a moving BEC has been demonstrated independently of quantized states or critical velocities ^{25,26}. Lastly, we note that unlike ferromagnetism, this energy structure is periodic in Ω with period Ω_0 , as shown in Fig. 1c. Similar periodic swallowtails are predicted for superfluids trapped in a lattice ¹⁹.

Our superfluid system is a BEC of ²³Na atoms in a ring-shaped optical dipole trap, as shown in Fig. 2a. To induce flow, a blue-detuned laser creates a rotating repulsive potential, depleting the density in a small portion of the ring and thereby creating a weak link ²⁷. The intensity of the laser sets the height of this potential, U . Without this weak link, superfluid flow in the ring should be quite stable ²⁴ with $\Omega_c^+ \gg \Omega_0$. Changing U will change the critical angular velocities Ω_c^\pm and the size of the hysteresis loop. Rotating the weak link in the azimuthal direction at angular frequency

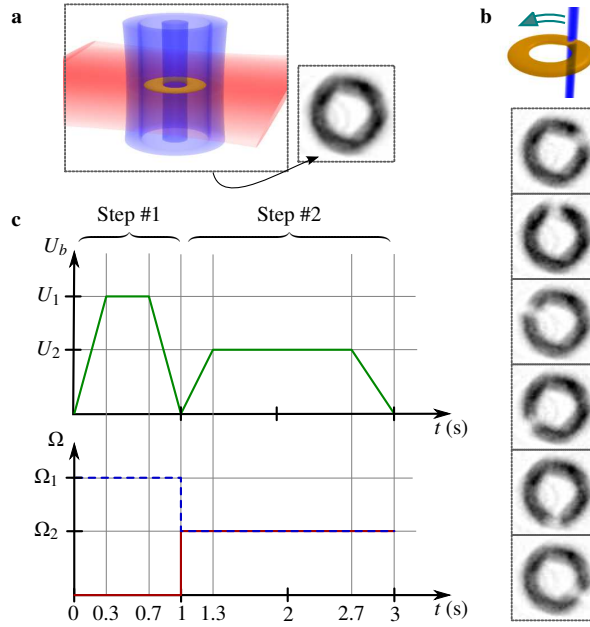


Figure 2: Experimental setup and procedure. **a**, Schematic and *in-situ* images of our trap, which is formed by crossing a ring-shaped dipole trap for radial confinement and a sheet trap for vertical confinement. **b**, Schematic and *in-situ* images of a ring stirred by a repulsive weak link. **c**, Two step experimental sequence: the height U of the repulsive potential and angular rotation rate Ω as a function of time. Step #1 sets the initial winding number using Ω_1 (either 0 Hz or 1.1 Hz) and U_1 ($\approx 1.1\mu_0$); step #2 probes the hysteresis with Ω_2 and U_2 (see text).

Ω , as shown in Fig. 2b, can drive transitions, or phase slips, between the quantized circulation states ⁸.

To observe hysteresis in these phase slips, we use a two step experimental sequence, as shown in Fig. 2c. After condensing the atoms into the ring trap, the BEC is prepared into either $n = 0$ or $n = 1$ circulation states by either not rotating the weak link or by rotating it at $\Omega_1 = 1.1$ Hz. The fidelity with which this procedure generates the expected initial state is $\gtrsim 97\%$. We then stir the weak link at various angular velocities Ω_2 for an additional 2 s. Ω_2 spans the range between -0.3 Hz and 1.2 Hz. In step #1, U is ramped to $U_1 \approx 1.1\mu_0$, where μ_0 is the global chemical potential. In step #2, U is ramped to a chosen U_2 . The transitions from $n = 0 \rightarrow 1$ and $n = 1 \rightarrow 0$ occur at different values of Ω_2 and form hysteresis loops, as Fig. 3a–f show. Each plot shows the measured hysteresis loop for a specific U_2 . As U_2 is increased, both Ω_c^+ and Ω_c^- become closer to $\Omega_0/2$, i.e., the hysteresis loop becomes smaller. The observed transitions are not sharp unlike those in Fig. 1b. The dominant broadening mechanism is likely shot-to-shot atom number fluctuations, but the non-zero temperature (≈ 100 nK) may also contribute (see Supplemental Material).

Fig. 3g shows the measured size of the hysteresis loop, $(\Omega_c^+ - \Omega_c^-)/\Omega_0$, as a function of the strength of the weak link; the size of the loop monotonically decreases with increasing U_2/μ_0 until it reaches a value consistent with zero near $U_2/\mu_0 \approx 0.75$. To predict the size of the hysteresis loop, we used two models. First, we used an effective one-dimensional model which, as a function of Ω_2 , computes the fluid velocity in the rotating frame. We assume that Ω_c^\pm will occur when this velocity reaches the local speed of sound ²⁸. As a separate approach, we also simulated our system

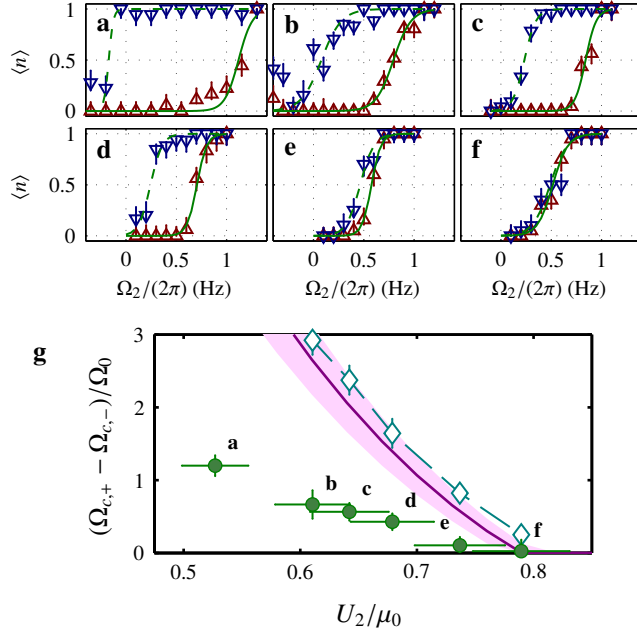


Figure 3: Hysteresis data. **a-f**, Hysteresis loops with sigmoid fits. The red triangle (blue inverted triangles) show the winding number n averaged over ≈ 20 shots, when starting with $n = 0$ ($n = 1$). All error bars show the 68% confidence interval. The fits determine Ω_c^\pm and $\Omega_0/2$ (gray, vertical lines; see Methods) and their uncertainties. **g**, Hysteresis loop size vs. U_2 . The green circles show the experimental data. The magenta line and band are the prediction and uncertainty of an effective 1D hydrodynamic model ²⁸. The open (filled) cyan diamonds and their uncertainties are the results of our GPE simulation with $\Lambda = 0$ ($\Lambda = 0.01$).

with the 3-D, time-dependent Gross-Pitaevskii equation (GPE). These two approaches predict hysteresis and are consistent, suggesting that both theories predict that Ω_c^\pm is determined by the sound speed. Despite occurring at the sound speed, the observed excitations in the GPE simulation are vortex/anti-vortex pairs. Perhaps most strikingly, Fig. 3g shows a large discrepancy between our models and experiment.

One property of the system that our models fail to include is dissipation. As another approach, we added dissipation to the GPE phenomenologically ²⁹,

$$i\hbar\frac{\partial\psi}{\partial t} = (1 - i\Lambda)\left[-\frac{\hbar^2}{2m}\nabla^2 + V(x, y, z, t) + gN|\psi|^2 - \mu\right]\psi, \quad (1)$$

where ψ is the BEC wavefunction, g is the interaction strength, V is the externally applied potential (trap and weak link), N is the atom number, μ is the chemical potential of the initial stationary state, and Λ is the dissipation parameter. With $\Lambda = 0.01$, a reasonable value for our experiment, the hysteresis loop size decreases as shown in Fig. 3g but not significantly compared to the discrepancy with experiment. Increasing the damping parameter further does not improve the agreement (see Supplemental Material). However, it is clear that dissipation is important. In fact, dissipation is essential and implicitly assumed in the energy landscape picture described in Fig. 1: dissipation allows the system to relax to the minima of the landscape; without dissipation, the system cannot change its energy.

To gain insight, we consider a toy model where the relevant excitations are vortex/anti-vortex pairs and derive the associated energy landscape. If a (anti-)vortex were to be nucleated at the (inner) outer edges (as shown in Fig. 4a), move to center, and annihilate, the winding number

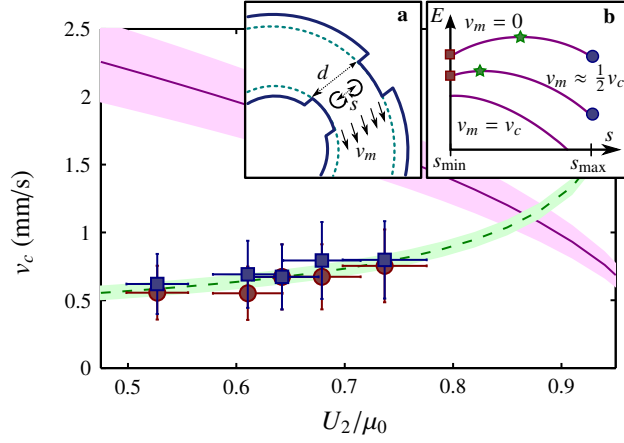


Figure 4: Extracted critical velocities vs. U_2 . The red circles (blue squares) show the critical velocities extracted from Ω_c^+ (Ω_c^-). The magenta line and band show the estimate and uncertainty of the local speed of sound. The green, dashed line and band show the best fit of the toy model of vortex creation and its statistical uncertainty. All uncertainties are 1σ . **a**, A diagram of a vortex/anti-vortex pair in a weak link of width d and a vortex/anti-vortex separation s . **b**, Energy landscape as a function of s for three different values of the velocity in the weak link region v_m , showing the stable states (\blacksquare, \bullet) and the energy barrier (\star).

would change by one unit. The energy of a vortex/anti-vortex pair in a perfectly hard-walled ring trap in the presence of a velocity field has been derived using the method of images³⁰. In the limit that the width of the annulus $d \ll R$, this energy reduces to

$$E = \pi\rho d R v^2 + 2\pi \frac{\hbar\rho s v}{m} + 2\pi \frac{\rho\hbar^2}{m^2} \ln \left[\frac{d}{\pi\xi} \sin \left(\frac{\pi s}{d} \right) \right], \quad (2)$$

where s is the separation between the vortices, v is the velocity of the superfluid, ρ is the effective 2D mass density, and ξ is the healing length of the condensate and therefore the core size. This equation applies to a system with a uniform annulus width d and uniform velocity v . To apply this model to our system, we take d to be the effective width of the annulus in the weak link region and $v = v_m$, the maximum velocity in the weak link. For $v_m = 0$, Eq. 2 has a maximum at $s = d/2$ while diverging negatively at d and 0. Such a divergence is unphysical, because the non-zero radii of the vortices prevent them from coming arbitrarily close to each other or the wall. We assume the distance of closest approach to the walls is $C\xi$ and between vortices is $2C\xi$, where C is of order unity. Thus, s ranges from $s_{\min} = 2C\xi$ to $s_{\max} = d - 2C\xi$. We assume that vortices annihilate at s_{\min} and enter the annulus at s_{\max} .

We plot the energy landscape described above in Fig. 4b for several different v_m and constant d . The two stable states, at s_{\min} and s_{\max} , represent a winding number difference of one. This implies that for a phase slip to occur the vortex pair must nucleate at either s_{\max} or s_{\min} and move to the opposite extreme. This happens when the energy barrier disappears, *i.e.*, when $dE/ds|_{s=s_{\min(\max)}} = 0$. This defines the critical velocity $v_m = v_c$ as

$$v_c = \pm \frac{\pi\hbar}{md} \cot \left(\pi \frac{2C\xi}{d} \right), \quad (3)$$

where $+(-)$ refers to starting at $s_{\min}(s_{\max})$.

To compare this model to our experiment, we computed the critical velocity in the weak link from the transitions in the hysteresis loops. The critical velocity is not a simple function of U_2/μ_0 and Ω_2 ; rather the requirements of quantized winding number and, in a frame co-rotating with the weak link, continuity of flow, require a self-consistent solution for the flow velocity around the entire ring (see Methods). Fig. 4 shows the result of this calculation. In direct contrast to the local speed of sound in the weak link, which decreases as $\sqrt{1 - U_b/\mu_0}$, we find that the critical velocity *increases*. The observed critical velocity is well fit to Eq. 3 with a single value of $2C\xi/d$. This value implies a distance of closest approach $2C\xi \approx 0.4d$. Over the region of interest, the value of C ranges from 1.5 to 0.7, agreeing with the assumption that it is of order unity (C is calculated using the best estimates of ξ and d , both of which vary with U). The fact that the data can be fit using this crude model suggests that vortices are the relevant excitations and Eq. 2 (or something that captures similar physics) gives a good prediction of the energy landscape.

Our hysteretic system has the essential features of the rf-SQUID. Just as SQUIDs detect magnetic fields, our analogous system can detect rotations. Hysteresis plays an important role in rf-SQUIDs, where it is used as a readout mechanism. In our system, hysteresis will also be important, allowing for greater accuracy by canceling systematic effects. The hysteresis loops are centered about $\pm\Omega_0/2$ for different directions of rotation; therefore, one can measure the asymmetry in the measurements of $\pm\Omega_0/2$ to extract an unknown bias rotation. Such measurements may cancel out effects like asymmetries in the ring potential.

In conclusion, we have measured hysteresis in a dilute atomic gas BEC, a phenomenon that is as fundamental to superfluidity as the existence of persistent currents and critical velocities. Our studies suggest that the elementary excitations involved in hysteresis are vortices and that dissipation plays an important role in the dynamics. We suspect that more sophisticated models that include dissipation will yield better agreement. Finally, beyond being an atomtronic rotation sensor, it is possible that in the hysteretic regime this device could act as classical memory or a digital noise filter in future atomtronic circuits.

Methods Summary The ring-shaped BEC, which contains approximately 4×10^5 ^{23}Na atoms, is created from a cloud of laser cooled atoms by evaporation, first in a magnetic trap and then in a ring-shaped optical dipole trap. The optical dipole trap is shaped roughly like a washer (see Methods), with measured harmonic trap frequencies in the vertical direction of 472(4) Hz and 188(3) Hz in the radial direction. (Uncertainties in this paper are the uncorrelated combination of 1σ statistical and systematic uncertainties unless stated otherwise.) The mean radius of the trap is 19.5(4) μm . The weak link is created by a blue-detuned laser beam (see Methods). Time of flight expansion of the condensate allows us to determine the winding number by measuring the size of the central hole size that appears in the cloud.

1. Pepino, R., Cooper, J., Anderson, D. & Holland, M. Atomtronic Circuits of Diodes and Transistors. *Phys. Rev. Lett.* **103**, 140405 (2009).
2. Beeler, M. C. *et al.* The spin Hall effect in a quantum gas. *Nature (London)* **498**, 201 (2013).

3. Silver, A. H. & Zimmerman, J. E. Quantum States and Transitions in Weakly Connected Superconducting Rings. *Phys. Rev.* **157**, 317–341 (1967).
4. Zimmerman, J. E. Design and Operation of Stable rf-Biased Superconducting Point-Contact Quantum Devices, and a Note on the Properties of Perfectly Clean Metal Contacts. *Journal of Applied Physics* **41**, 1572 (1970).
5. Mueller, E. J. Superfluidity and mean-field energy loops: Hysteretic behavior in Bose-Einstein condensates. *Phys. Rev. A* **66**, 63603 (2002).
6. Ramanathan, A. *et al.* Superflow in a Toroidal Bose-Einstein Condensate: An Atom Circuit with a Tunable Weak Link. *Phys. Rev. Lett.* **106**, 130401 (2011).
7. Moulder, S., Beattie, S., Smith, R. P., Tammuz, N. & Hadzibabic, Z. Quantized supercurrent decay in an annular Bose-Einstein condensate. *Phys. Rev. A* **86**, 013629 (2012).
8. Wright, K. C., Blakestad, R. B., Lobb, C. J., Phillips, W. D. & Campbell, G. K. Driving Phase Slips in a Superfluid Atom Circuit with a Rotating Weak Link. *Phys. Rev. Lett.* **110**, 25302 (2013).
9. Onofrio, R., Raman, C. & Vogels, J. Observation of superfluid flow in a Bose-Einstein condensed gas. *Phys. Rev. Lett.* **85**, 2228–31 (2000).
10. Inouye, S. *et al.* Observation of Vortex Phase Singularities in Bose-Einstein Condensates. *Phys. Rev. Lett.* **87**, 080402 (2001).

11. Engels, P. & Atherton, C. Stationary and Nonstationary Fluid Flow of a Bose-Einstein Condensate Through a Penetrable Barrier. *Phys. Rev. Lett.* **99**, 160405 (2007).
12. Miller, D. *et al.* Critical Velocity for Superfluid Flow across the BEC-BCS Crossover. *Phys. Rev. Lett.* **99**, 070402 (2007).
13. Neely, T. W., Samson, E. C., Bradley, a. S., Davis, M. J. & Anderson, B. P. Observation of Vortex Dipoles in an Oblate Bose-Einstein Condensate. *Phys. Rev. Lett.* **104**, 160401 (2010).
14. Desbuquois, R. *et al.* Superfluid behaviour of a two-dimensional Bose gas. *Nat Phys* **8**, 645–648 (2012).
15. Albiez, M. *et al.* Direct Observation of Tunneling and Nonlinear Self-Trapping in a Single Bosonic Josephson Junction. *Phys. Rev. Lett.* **95**, 010402 (2005).
16. Levy, S., Lahoud, E., Shomroni, I. & Steinhauer, J. The a.c. and d.c. Josephson effects in a Bose-Einstein condensate. *Nature (London)* **449**, 579–583 (2007).
17. Diakonov, D., Jensen, L., Pethick, C. & Smith, H. Loop structure of the lowest Bloch band for a Bose-Einstein condensate. *Phys. Rev. A* **66**, 013604 (2002).
18. Watanabe, G., Yoon, S. & Dalfovo, F. Swallowtail Band Structure of the Superfluid Fermi Gas in an Optical Lattice. *Phys. Rev. Lett.* **107**, 270404 (2011).
19. Morsch, O. & Oberthaler, M. Dynamics of Bose-Einstein condensates in optical lattices. *Rev. Mod. Phys.* **78**, 179–215 (2006).

20. Kojima, H., Veith, W., Putterman, S., Guyon, E. & Rudnick, I. Vortex-Free Landau State in Rotating Superfluid Helium. *Phys. Rev. Lett.* **27**, 714 (1971).
21. Schwab, K., Bruckner, N. & Packard, R. Detection of the Earth's rotation using superfluid phase coherence. *Nature (London)* **386**, 585 (1997).
22. Schwab, K., Bruckner, N. & Packard, R. The superfluid ^4He analog of the RF SQUID. *J. Low Temp. Phys.* **110**, 1043–1104 (1998).
23. Plischke, M. & Bergersen, B. *Equilibrium Statistical Physics* (World Scientific, Singapore, 2006), 3rd edn.
24. Baharian, S. & Baym, G. Bose-Einstein condensates in toroidal traps: Instabilities, swallow-tail loops, and self-trapping. *Phys. Rev. A* **87**, 13619 (2013).
25. Recati, A., Zambelli, F. & Stringari, S. Overcritical Rotation of a Trapped Bose-Einstein Condensate. *Phys. Rev. Lett.* **86**, 377–380 (2001).
26. Madison, K., Chevy, F., Bretin, V. & Dalibard, J. Stationary States of a Rotating Bose-Einstein Condensate: Routes to Vortex Nucleation. *Phys. Rev. Lett.* **86**, 4443–4446 (2001).
27. Hoskinson, E., Sato, Y., Hahn, I. & Packard, R. E. Transition from phase slips to the Josephson effect in a superfluid ^4He weak link. *Nat Phys* **2**, 23–26 (2006).
28. Watanabe, G., Dalfovo, F., Piazza, F., Pitaevskii, L. P. & Stringari, S. Critical velocity of superfluid flow through single-barrier and periodic potentials. *Phys. Rev. A* **80**, 53602 (2009).

29. Choi, S., Morgan, S. & Burnett, K. Phenomenological damping in trapped atomic Bose-Einstein condensates. *Phys. Rev. A* **57**, 4057–4060 (1998).
30. Fetter, A. L. Low-Lying Superfluid States in a Rotating Annulus. *Phys. Rev.* **153**, 285–296 (1967).

Supplementary Information is available in the online version of the paper.

Acknowledgements This work was partially supported by ONR, the ARO atomtronics MURI, NIST, the NSF through the PFC at the JQI and grant PHY-1068761. S.E. is supported by a National Research Council postdoctoral fellowship. We wish to thank K. Wright, W. T. Hill, III, and A. Kumar for valuable discussions and experimental assistance.

Author Contributions S.E, J.G.L and F.J took the experimental data. N.M, C.W.C and M.E developed and performed the GPE simulations. All authors were involved in analysis and discussions of the results, and contributed to writing the manuscript.

Author Information Reprints and permissions information is available at www.nature.com/reprints. The authors declare no competing financial interests. Correspondence and requests for materials should be addressed to G.K.C. (gretchen.campbell@nist.gov).

Methods

Optical dipole traps. Our optical dipole trap is formed by the combination of two laser beams. A blue-detuned ($\lambda = 532$ nm) laser beam passes through a ring-shaped intensity mask, and the

shadow is imaged onto the atoms forming a repulsive, ring-shaped potential. This trap combines with an attractive confining potential in the vertical direction, generated by a red-detuned ($\lambda = 1064$ nm) laser beam shaped like a sheet. If the imaging resolution were perfect, the trap would be hard-walled in the radial direction, but it is in fact closer to a Gaussian with $1/e^2$ radius of $8.9(9)$ μm .

To create the weak link, an acoustic optical deflector elongates a blue-detuned, focused, Gaussian beam by scanning radially at 2 kHz. The beam was turned on and off with a 300 ms linear ramp. The $1/e^2$ half-width of the weak link along the azimuthal direction is approximately 6 μm , limited by the resolution of our imaging system. The size of the weak link along the radial direction is $\approx 50\%$ larger than the Thomas-Fermi width of the BEC.

We calibrated the weak link by observing the atomic density depletion caused by the weak link potential (see Supplemental Material). The dominant uncertainty in U_2/μ_0 is in the common calibration and is reflected in the horizontal error bars in Figs. 3 & 4; the relative uncertainties between the points are smaller.

BEC parameters. Approximately 4×10^5 atoms comprise the BEC after evaporation first in a magnetic time orbiting potential (TOP) trap and subsequently in the optical traps described above. We estimate the global chemical potential μ_0 to be $\mu_0/\hbar \approx 2\pi \times (1.7$ kHz) and the corresponding Thomas-Fermi full width in the vertical (radial) direction to be 3.2 μm (8.1 μm). Given this mean radius, we expect $\Omega_0 = 1.19(4)$ Hz, in rough agreement with the measured value of $\Omega_0 = 1.05(5)$ Hz (by assuming the hysteresis loops are centered on $\Omega_0/2$).

Measurement of the winding number. To measure the final rotational state after stirring, the BEC is released from the trap and imaged after 10 ms of time-of-flight (TOF). As the BEC expands, rotation will cause a hole to appear in the center. As with the winding number, the size of this feature is quantized and enables determination of the final circulation state ^{7,8}. Direct release from the repulsive dipole trap does not allow the hole to be resolved in 10 ms TOF, so we transfer first to an attractive ring and apply a decompression procedure similar to that of Wright, *et al.* ⁸, before using partial transfer absorption imaging [?].

Estimating the uncertainty in the average winding number. Given that the outcome of any given experiment is either $n = 0$ or $n = 1$, traditional methods of estimating the uncertainty in the mean value (e.g., Gaussian statistics) are not applicable. The uncertainty in this average can be estimated by the cumulative beta distribution, which is appropriate for experiments that yield binary results [?].

Fitting the hysteretic transitions and determining Ω_c^\pm and its uncertainty. We use a sigmoid of the form $1/[\exp\{-(\Omega_2 - \Omega_t)/\delta\Omega\} + 1]$ to fit the data as in Fig. 3, where Ω_t and $\delta\Omega$ are the fit parameters. While this fit well describes the data, the relationship between Ω_c^\pm and the fit parameters depends on the mechanisms for the broadening of the transition. For example, consider a model where thermal fluctuations drive the system over the energy barrier. This would occur when the energy barrier becomes of the order of $k_B T$, where k_B is the Boltzmann constant and T is the absolute temperature. The dynamics of this process are random and would lead to phase slips at lower values of Ω_2 for $0 \rightarrow 1$ transition (and higher values for $1 \rightarrow 0$ transitions). In principle, this effect would cause a broadening of the transition region, and the zero temperature Ω_c^\pm would then

correspond to the value of Ω_2 where probability for a transition equals unity. However, a different mechanism could be responsible for the broadening. In particular, atom number fluctuations can change U_2/μ_0 , and therefore Ω_c^\pm , from shot to shot. On average, this leads to a broadening. Based on the experimentally observed change in the Ω_c^\pm vs. the strength of the weak link and our atom number shot to shot fluctuations of $\approx 16\%$ (this represents the peak-to-peak fluctuations for 95% of the data), we expect the transitions to be approximately 0.12 Hz wide, compared to the average of 0.18 Hz. Because atom number fluctuations explain most of the width, we take $\Omega_c^\pm = \Omega_r$, and, to account for the possibility of finite temperature or other unknown broadening effects, take the 1σ uncertainty to be $\frac{3}{2}\delta\Omega$.

Extracting the critical velocity. Extracting the critical velocity in our system is non-trivial because the flow must satisfy the requirements of quantized winding number and continuity of flow in the frame rotating with the weak link. (Continuity of flow does not occur in any other frame.) One counterintuitive result of these requirements is that moving the weak link will impart some angular momentum to the superfluid as viewed from the fixed, laboratory frame even in the $n = 0$ state^{?,20}. To extract the critical velocity given these constraints, we work in the rotating frame. The velocity v_r of atoms in the rotating frame is related to the rotation rate of the weak link by

$$\frac{m}{\hbar} \int_0^{2\pi} v_r(\theta) R d\theta + 2\pi \frac{\Omega}{\Omega_0} = 2\pi n, \quad (4)$$

where θ is the azimuthal angle. This equation is an expression of the Bohr-Sommerfeld quantization condition. The first term represents the phase accumulated by the atoms after integrating once around the ring and the second term represents the Sagnac (Peierls) phase that appears due to transforming into the rotating frame. In the rotating frame, the velocity $v_r(\theta)$ and the mass density $\rho(\theta)$

satisfies a continuity equation: $\rho(\theta_1)v_r(\theta_1) = \rho(\theta_2)v_r(\theta_2)$, where θ_1 and θ_2 are any two azimuthal angles. Given a U_2/μ_0 , we determine the equivalent 1D density $\rho(\theta)$ by integrating over the radial and vertical directions of our cloud using the Thomas-Fermi approximation. For a given rotation rate Ω and density $\rho(\theta)$, Eq. 4 and the continuity equation determine $v_r(\theta)$ and, in particular, the velocity in the weak link $v_m = \max[v_r(\theta)]$ uniquely. The critical velocity is then taken to be the value of v_m when the weak link is rotated at the critical rotation rate Ω_c^\pm .

When $\Omega_c^+ - \Omega_c^- \rightarrow 0$, this method of extracting v_c is unreliable and thus we neglect the point near $U \approx 0.8\mu_0$ (see Supplemental information). Going slightly further into the regime where $U > \mu_0$ results in the BEC being broken.